New approach to the compound energy formalism (NACEF) Part II. Thermodynamic modelling of the Al–Nb system supported by first-principles calculations

J.M. Fiorani, M. Badran, J.M. Joubert, J.C. Crivello, A.A.A.P. da Silva, G.C. Coelho, C.A. Nunes, Nicolas David, M. Vilasi

New Approach to the Compound Energy Formalism (NACEF)
Part II. Thermodynamic modelling of the Al–Nb system supported by first-principles calculations

J.M. Fiorani[a,*], M. Badran[a], J.M. Joubert[b], J.C. Crivello[b], A.A.A.P da Silva[c], G.C. Coelho[d], C.A. Nunes[d], N. David[a], M. Vilasi[a]

[a] Univ. de Lorraine, CNRS, Institut Jean Lamour, UMR 7198, Campus ARTEM, 2 allée André Guinier, 54011 Nancy, France

[b] Univ. Paris Est Créteil, CNRS, ICMPE, UMR 7182, 2 rue Henri Dunant, 94320 Thiais, France

[c] IEM/UNIFEI – Instituto de Engenharia Mecânica,Universidade Federal de Itajubá, Avenida BPS 1303, Itajubá, 37500-903, Brazil

[d] Escola de Engenharia de Lorena - EEL, Universidade de São Paulo – USP, Estrada Municipal do Campinho, 12600-000, Lorena, SP, Brasil

[*] Corresponding author. E-mail address: jean-marc.fiorani@univ-lorraine.fr (J.M. Fiorani)

Keywords:
Thermodynamic modelling
Al–Nb
CALPHAD
New Approach to the Compound Energy Formalism (NACEF)
Ab initio calculations
σ phase

ABSTRACT

In the present work, a new assessment of the Al–Nb system, using a combined first-principle and CALPHAD approach, is presented. Formation enthalpies of all ordered configurations of the intermetallic phases (σ, $D0_{22}$ and $A15$) were estimated from ab initio calculations. The liquid, fcc and bcc phases are described by a substitutional solution model. The intermetallic phases $D0_{22}$ and $A15$ are described with the New Approach to the Compound Energy Formalism (NACEF). To model the σ phase, four descriptions are applied. In first, σ phase is described with the five-sublattice (5SL) model using combined CEF model

where a modification was applied which allows to respect the formation enthalpies of end-members obtained from ab initio calculations. Then, a comparison with the results obtained using the NACEF approach applied to the five-sublattice (5SL), three-sublattice (3SL) and two-sublattice (2SL) models is presented. In all cases, assessments derived from the different descriptions of σ phase show very good agreement with the available experimental and ab initio data with a limited number of used parameters. In this sense, self-consistent thermodynamic descriptions of the Al–Nb system is provided. Moreover, this work shows from the example of the σ phase that the NACEF approach, contrary to what is commonly considered, allows the compatibility between different descriptions using different numbers of sublattices. This is particularly interesting for the construction of multi-component databases.

1. Introduction

The Al-Nb system is an important binary system for the development of many structural materials or as coatings for high temperature applications. Based on inconsistencies between the most recent assessments [1,2] as well as data from heat-treated ternary alloys [2–5] containing Nb and Al, new investigations on the solubility limits of the intermetallic phases of the Al–Nb system were recently reevaluated by [6] via Electron Probe MicroAnalysis – Wavelength Dispersive Spectrometry (EPMA – WDS) from equilibrated alloys.

In the last decade, First Principles (FP) calculation methods have complemented the experimental data as an important source of input for thermodynamic assessments. In this way, the total energies of all end-member compounds were calculated in the present work for *A*15 (Nb_3Al), σ (Nb_2Al) and $D0_{22}$ ($NbAl_3$) phases. The electronic structure and total energy calculations were based on Density Functional Theory (DFT). The purpose of the present work is to provide an accurate thermodynamic description for the Al–Nb system taking into account the new experimental data given by [6] and using results from DFT calculations for compounds within the CALPHAD framework.

In a previous article [7] which composes the first part of the present study, it has been shown that the NACEF Formalism constitutes a promising way to improve the capacity of the CEF to describe simple or complex phases. In the present article, the NACEF approach is applied to the modeling of the Al-Nb system in order to illustrate its implementation.

2. Literature review

2.1 Phase equilibria data

Due its considerable industrial importance, the Al–Nb system has been investigated experimentally by many authors. Table 1 summarizes the experimental data available for the Al–Nb system concerning solidus/liquidus temperatures, phase solubility ranges, activity data and enthalpies of formation. The early studies of this system [8–14] are all in relatively good agreement in terms of phase stability. Besides the terminal phases, the *A*15, σ and $D0_{22}$ compounds are reported as stable (see Table 2 for crystallographic information).

The congruent formation of $D0_{22}$ is well established, however, there have been some discrepancies about the nature of formation of the other phases. For example, σ is reported to be formed either congruently [11] or peritectically [10,12,13]. The Al-rich side of this system is characterized by a degenerated equilibrium in which the liquid, $D0_{22}$ and (Al) phases are involved. This invariant reaction has been reported either as eutectic [10,11] or peritectic [8,9,12].

The most complete experimental work on the Al–Nb system was carried out by Jorda et al. [15]. In this paper, the authors determined the phase solubility ranges via metallography, XRD and EPMA analysis of samples heat-treated from 24 hours up to 1 month depending on the temperature of heat treatment. The authors also used levitation thermal analysis (LTA) and differential thermal analysis (DTA) to determine the temperature of the invariant reactions, solidus and liquidus lines, and the peritectic nature of the $D0_{22}$ and σ formation was confirmed. The solubility limits of the phases were also indirectly determined by Kokot et al. [16] via XRD analysis of arc-melted samples heat-treated for 14 days at 1100 °C and Menon et al. [17] via EPMA measurements of arc-melted alloys heat-treated at 1650 °C/50 h and subsequently heat treated at 1200 °C/14 days or 1000 °C/30 days. Shilo et al. [18] measured the variation of vapor pressure of Al according to the composition from binary alloys and indirectly determined the solubility limits of the phases. Their samples were previously heat treated at 1297 °C for 12 hours and then the vapor pressures were measured at 1571, 1607, 1672, 1721 °C with different durations and heating/cooling cycles.

Zhu et al. [19] performed Differential Scanning Calorimetry (DSC) measurements with different scanning rates from heat treated samples in order to determine the nature of the Al-rich equilibrium involving liquid, $D0_{22}$ and (Al). The suggested temperature was 661.44 °C, leading to a peritectic type reaction because it is slightly higher than the melting point of pure Al (660.3 °C). Witusiewicz et al. [1] performed new experiments (DTA and Pirani-Alterthum method) aiming at the determination of the high temperature solidus and liquidus lines. In general, their results are in good agreement with previous information [15]. Witusiewicz et al. [1] also measured the temperature of the degenerated Al-rich reaction as 657 °C ± 5 (DTA). More recently, Stein et al. [20] measured the $D0_{22}$ phase congruent melting temperature via DTA.

2.2 Thermodynamic data

All the thermodynamic data are summarized in Table 1. Several studies present estimated data for enthalpies of formation of the Al–Nb compounds based both on calculations as well as on experimental results. Meschel and Kleppa [22] and Mahdouk et al. [23] conducted experiments of Direct Reaction Calorimetry (DRC). Shilo et al. [18] carried out vapor pressure measurements in the high-temperature range 1844-2146 K using the Knudsen Effusion (KE) method aiming the determination of enthalpy of formation of the intermetallic compounds. George et al. [24] performed Electromotive Force (EMF) measurements in the intermediate temperature (973 to 1078 K) range by using solid-state electrochemical cells and CaF_2 as solid electrolyte. George et al. [24] and Shilo et al. [18] also have measured the activities of Al in the Al–Nb system.

From FP calculations, formation enthalpies for the three intermetallic phases were also obtained by Colinet et al. [25], Watson et al. [26], Papadimitriou et al. [27] and Pisch [28] for the $D0_{22}$ phase.

2.3 CALPHAD modeling

The Al–Nb system was firstly described according to the CALPHAD methodology by Kaufman and Nesor [29], considering all compounds as stoichiometric. Later, it was reassessed by Kaufman [30] where the σ phase was modeled as a substitutional solid solution. Subsequent studies have modeled the *A*15 phase either as $(Nb)_3(Al,Nb)_1$ [1,19,31,32] or $(Al,Nb)_3(Al,Nb)_1$ [1,33], the σ phase mostly as $(Nb)_4(Al,Nb)_{16}(Nb,Al)_{10}$ and the $D0_{22}$ phase has been modeled as either stoichiometric [19,31] or $(Al,Nb)_1(Al,Nb)_3$ [1,8,32,33]. Table 3 summarizes the sublattice models applied in the descriptions of these intermetallic phases used in the assessments of the various authors cited above.

Considering the two most recent modelings [1,2], one can notice that they are based on a simplified description of the σ phase and on a set of relatively few thermodynamic data. Moreover, comparisons with the phase diagram data given in Fig. 1 show that the solubilities are rather badly respected and more particularly in the case of the σ phase. This is the reason why we present in this work a new modeling of the Al-Nb system using DFT calculations.

3. First-principle calculations

It has become customary to use data from DFT calculations for the Gibbs energy in CALPHAD description in order to supplement the experimental information [34] and to provide data in metastable composition range. In the present work, the first principles method has been used to express the 0 K heat of formation of every configurations generated by the distribution of every atoms in the different sublattices of the considered phase (here: σ, *A*15, $D0_{22}$). Present calculations are based on the density functional theory (DFT), were carried out using the VASP package [35,36]. The generalized gradient approximation (GGA) was used with the Perdew-Burke-Ernzerhof (PBE) exchange and correlation energy functional [37,38]. An energy cutoff of 400 eV was used for the plane wave basis set within a high density mesh of $2\pi \cdot 0.05/Å$ units for each direction of the irreducible Brillouin generated by the Monkhorst-Pack procedure [39]. The conditions for the calculation (relaxation method, convergence accuracy) have been detailed previously [40]. All the calculations have been handled using the ZenGen code [41], for the generation of input files, the job monitoring and results analysis.

The total energies for all the end-members of σ, *A*15 and $D0_{22}$ phases were calculated and the corresponding enthalpies of formation referred to fcc Al and bcc Nb are reported in Tables 4, 5 and 6 respectively and are plotted in Fig. 2. The intermediate phase $D0_{22}$ whose structure is a fcc closed-packed superlattice [42] has a narrow range of stability around the stochiometric composition. Moreover, $D0_{22}$ is body-centred tetragonal and ab initio calculations [25,43] suggest that fcc Nb is mechanically unstable with respect to tetragonal distortions. Consequently, only the two ordered configurations $Al^{2b}Al^{4d}Nb^{2a}$ and

$Nb^{2b}Nb^{4d}Al^{2a}$ were considered (see Table 6). To consider the order-disorder transition $D0_{22}$-$A1$ in the present work, values of Al and Nb elements in the $A1$ structure taken from the SGTE database are considered for the pure components in the $D0_{22}$ structure. When modeling the order-disorder transition $D0_{22}$-$A1$, the FCC phase and the disordered state of the $D0_{22}$ phase have the same Gibbs energy and therefore cannot be discerned in the calculation of the equilibria. To remedy this, we attribute (see Table 6) a slightly positive value (1 J/mol to the pure elements in the $D0_{22}$ structure) to the $D0_{22}$ phase so that the FCC phase is privileged.

4. Thermodynamic models

4.1 Solution phases

The Gibbs energy for the solution phases φ, liquid, $A1$ and $A2$ are described by the substitutional solution model with Redlich–Kister polynomials for the excess Gibbs energy contribution:

$$G^{\varphi} = \sum_i x_i {}^0G_i^{\varphi} + RT\sum_i x_i \ln x_i + x_i x_j \sum_{\upsilon=0} \left(x_i - x_j\right)^{\upsilon} {}^{\nu}L_{i,j}^{\varphi} \quad (1)$$

where x_i represent the mole fraction of the elements i and ${}^0G_i^{\varphi}$ is the Gibbs energy of the pure elements in the structure of phase φ. ${}^{\nu}L_{\mathrm{Al,Nb}}^{\varphi}$, are the Redlich-Kister parameters representing the interaction of order ν between components Al and Nb in the φ phase and are linear functions of temperature with adjustable parameters.

4.2 Compounds ($A15$ and $D0_{22}$ and σ phases)

For the description of ordered phases with the CEF [44] or the NACEF approach [7], a sublattice is introduced for each Wyckoff sites in the crystal structure. $A15$ and $D0_{22}$ phases are both modeled by the 2SL model $(Al,Nb)_3(Al,Nb)_1$ and using the NACEF approach [7]. Note that this means that for the $D0_{22}$ compound, the two sites 2*b* and 4*d* are merged (see Table 2). Since the intermediate phase $D0_{22}$ has a structure which is a fcc closed-packed superlattice [42], the order-disorder transition $D0_{22}$-$A1$ has been taken into account in the present work thanks to the NACEF approach.

The σ phase is an important intermetallic compound which exists in many binary systems and has been reviewed by Joubert [45]. The unit cell of the σ phase consists in 30 atoms arrayed in five distinct crystallographic positions (see Table 2), corresponding to five sublattices with 2, 4, 8, 8, 8 multiplicities, respectively. Due to its crystallographic complexity, the choice of a thermodynamic model for the σ phase remains troublesome. Ideally, all five different crystallographic sublattices should be considered in the thermodynamic model. Furthermore chemical substitution needs to be allowed on all sublattices [45]. However, the five-sublattice model (5SL) $(Al,Nb)_2^{2a}(Al,Nb)_4^{4f}(Al,Nb)_8^{8i_1}(Al,Nb)_8^{8i_2}(Al,Nb)_8^{8j}$ leads to too many parameters to be optimized in multi-component systems. A series of models have been proposed for the

description of the σ phase where sites of the crystal structure can be combined into a smaller set of sublattices based on site occupation data and coordination numbers for simplified model descriptions [45–47]. As in the Al–Nb system (see Table 3), the three-sublattice model $(\mathrm{Nb})_{4}^{4f}(\mathrm{Al,Nb})_{16}^{8i_1+8j}(\mathrm{Al,Nb})_{10}^{2a+8i_2}$ which is based on the recommendation by Ansara et al. [47] was commonly used as a reasonable simplification of the 5SL model to reduce the number of end-members. Unfortunately, using this simplified three-sublattice model, some difficulties were met to describe the σ phase accurately in terms of the compositional range and physical properties. Joubert [45] and Mathieu et al. [46] investigated simplifications for the σ phase sublattice models, evaluating the best agreement with the experimental data. In order to respect the crystal structure and the nature of the defects in this phase, these authors recommend as simplifications the three-sublattice (3SL) model $(\mathrm{Al,Nb})_{4}^{4f}(\mathrm{Al,Nb})_{16}^{8i_1+8j}(\mathrm{Al,Nb})_{10}^{2a+8i_2}$ where random mixing occurs in all sublattices and also the use of the two-sublattice (2SL) model $(\mathrm{Al,Nb})_{20}^{4f+8i_1+8j}(\mathrm{Al,Nb})_{10}^{2a+8i_2}$.

In the present work, four descriptions of the σ phase were established. On the one hand, the NACEF approach [7] was used to model the σ phase with the 5SL, 3SL and 2SL models. These three versions are named respectively σ-NACEF-5SL, σ-NACEF-3SL and σ-NACEF-2SL thereafter. On the other hand, the 5SL model based on the combined CEF model proposed by [48,49] was also used and the corresponding version is named σ -CEF-5SL.

4.2.1 NACEF description (σ-NACEF-5SL, σ-NACEF-3SL and σ-NACEF-2SL)

In the CEF approach, the Gibbs energy of a binary phase described with the sublattice model is given by different contributions which are functions of the site fractions $y_i^{(s)}$ of the different constituents *i* in the different sublattices *s*.

In NACEF formalism, site fractions are separated into two parts:

$$y_i^{(s)} = (y_i^{(s)} - x_i) + x_i \tag{2}$$

where $(y_i^{(s)} - x_i)$ is the ordering part which is equal to zero when the phase is disordered.

In the first part of the present work [7], it has been shown that all the ordered configurations result from different ordering into two sublattices Cn and that all the ordering parts $(y_i^{(s)} - x_i)$ can be expressed from the corresponding LRO parameters ηCn

Consequently, the Gibbs energy expressed by the CEF can be rewritten in the following form:

$$G^{SL} = {}^{\mathrm{Cfg}}G(y) + {}^{\mathrm{Ref}}G + {}^{\mathrm{Ex}}G^{\mathrm{dis}}(x) + \sum_{n=1}^{z} {}^{\mathrm{Ex}}G^{\mathrm{ord}}(\eta Cn) \tag{3}$$

$${}^{\mathrm{Cfg}}G(y) = \frac{RT}{\sum_s a^{(s)}} \sum_s a^{(s)} \sum_i y_i^{(s)} \ln y_i^{(s)} \tag{4}$$

$${}^{\mathrm{Ref}}G = \sum_i x_i \, {}^{0}G_i \tag{5}$$

$${}^{\mathrm{Ex}}G^{\mathrm{dis}}(x) = x_A x_B \sum_{\nu=0}^{s-2} (x_A - x_B)^{\nu} P\nu \tag{6}$$

$$^{Ex}G^{ord}(\eta Cn) = \sum_{\lambda=1}^{s} \eta Cn^{\lambda} \sum_{\mu=0}^{s-\lambda} (x_A - x_B)^{\mu} CnP\lambda\mu \qquad (7)$$

with z = 1, 3, 7 and 15 for s = 2, 3, 4 and 5 sublattices respectively. $^{0}G_i$ is the molar Gibbs energy of constituent i in the structure of the considered phase.

In NACEF form, the excess Gibbs energy is composed of a disordered part $^{Ex}G^{dis}(x)$ expressed in a Redlich-Kister form and an ordered part which is the sum of the different possible contributions $^{Ex}G^{ord}(\eta Cn)$ which are functions of the LRO parameters ηCn.

$P\nu$ and $CnP\lambda\mu$ are the NACEF parameters of the disordered and ordered excess parts respectively and are deduced from the CEF parameters:

$$\begin{bmatrix} P\nu \\ CnP\lambda\mu \end{bmatrix} = [\mathrm{Q}] . \begin{bmatrix} \mathrm{CEF} \\ \mathrm{parameters} \end{bmatrix} \qquad (8)$$

Note that the degree of the NACEF parameters which is given by ν or $\lambda + \mu$ depends on that of the CEF parameters considered. As example, an end-members $^{0}G_{i:j:k:l:m}$ in a five sublattice model implies NACEF parameters of the fifth degree.

In the NACEF approach, the corresponding parameters are optimized independently. This leads to express the CEF parameters from the NACEF parameters:

$$\begin{bmatrix} \mathrm{CEF} \\ \mathrm{parameters} \end{bmatrix} = [\mathrm{P}] . \begin{bmatrix} P\nu \\ CnP\lambda\mu \end{bmatrix} \qquad (9)$$

The matrix $[\mathrm{P}]$ thus defined is dependent of the number of sublattices s and of their site multiplicities.

The fourth degree constitutes a limitation for the development of the NACEF parameters which is only due to the need to express them from the CEF parameters. Indeed, beyond the fourth degree, the NACEF parameters become more numerous than the CEF parameters. Consequently, the general case given by the previous equation reduces as follows for 2, 3 and 5 sublattice models:

$$\begin{bmatrix} L_{A,B:A,B} \\ {}^{2}L_{A,B:*} \\ {}^{2}L_{*:A,B} \\ {}^{1}L_{A,B:A} \\ {}^{1}L_{A,B:B} \\ {}^{1}L_{A:A,B} \\ {}^{1}L_{B:A,B} \\ {}^{0}L_{A,B:A} \\ {}^{0}L_{A,B:B} \\ {}^{0}L_{A:A,B} \\ {}^{0}L_{B:A,B} \\ G_{AB} \\ G_{BA} \end{bmatrix} \text{ or } \begin{bmatrix} L_{A,B:A,B:*} \\ L_{A,B:*:A,B} \\ L_{*:A,B:A,B} \\ {}^{2}L_{A,B:*:*} \\ {}^{2}L_{*:A,B:*} \\ {}^{2}L_{*:*:A,B} \\ {}^{1}L_{A,B:i:j} \\ {}^{1}L_{i:A,B:j} \\ {}^{1}L_{i:j:A,B} \\ {}^{0}L_{A,B:i:j} \\ {}^{0}L_{i:A,B:j} \\ {}^{0}L_{i:j:A,B} \\ G_{ijk} \end{bmatrix} \text{ or } \begin{bmatrix} L_{A,B:A,B:*:*} \\ L_{A,B:*:A,B:*} \\ L_{A,B:*:*:A,B} \\ L_{A,B:*:*:*:A,B} \\ L_{*:A,B:A,B:*} \\ L_{*:A,B:*:A,B} \\ L_{*:A,B:*:*:A,B} \\ L_{*:*:A,B:A,B:*} \\ L_{*:*:A,B:*:A,B} \\ L_{*:*:*:A,B:A,B} \\ {}^{2}L_{A,B:*:*:*} \\ {}^{2}L_{*:A,B:*:*} \\ {}^{2}L_{*:*:A,B:*} \\ {}^{2}L_{*:*:*:A,B} \\ {}^{1}L_{A,B:i:j:k:l} \\ {}^{1}L_{i:A,B:j:k:l} \\ {}^{1}L_{i:j:A,B:k:l} \\ {}^{1}L_{i:j:k:A,B:l} \\ {}^{1}L_{i:j:k:l:A,B} \\ {}^{0}L_{A,B:i:j:k:l} \\ {}^{0}L_{i:A,B:j:k:l} \\ {}^{0}L_{i:j:A,B:k:l} \\ {}^{0}L_{i:j:k:A,B:l} \\ {}^{0}L_{i:j:k:l:A,B} \\ G_{ijklm} \end{bmatrix} = \left[\mathrm{P}^{DIS} \right] . \begin{bmatrix} P0 \\ P1 \\ P2 \end{bmatrix} + \sum_{n=1}^{z} \left[\mathrm{P}^{Cn} \right] . \begin{bmatrix} CnP10 \\ CnP11 \\ CnP12 \\ CnP13 \\ CnP20 \\ CnP21 \\ CnP22 \\ CnP30 \\ CnP31 \\ CnP40 \end{bmatrix} \tag{10}$$

and this leads to the following excess contributions:

$${}^{\mathrm{Ex}}G^{\mathrm{dis}}(x) = x_A x_B \left(P0 + P1(x_A - x_B) + P2(x_A - x_B)^2 \right) \tag{11}$$

$$\begin{aligned} {}^{\mathrm{Ex}}G^{\mathrm{ord}}(\eta Cn) = {} & \eta Cn \left[CnP10 + CnP11(x_A - x_B) + CnP12(x_A - x_B)^2 + CnP13(x_A - x_B)^3 \right] \\ & + \eta Cn^2 \left[CnP20 + CnP21(x_A - x_B) + CnP22(x_A - x_B)^2 \right] \\ & + \eta Cn^3 \left[CnP30 + CnP31(x_A - x_B) \right] \\ & + \eta Cn^4 \left[CnP40 \right] \end{aligned} \tag{12}$$

However, it should be noted that a development of degree less than or equal to 4 turns out to be sufficient in the vast majority of cases to describe the phases by the NACEF approach as it is shown in the present work for the description of the sigma phase with a 5SL model.

Moreover, it should be noted from Eq. (63) that in the NACEF approach, the energy of formation of the different compounds are function of the NACEF parameters and

consequently, the corresponding DFT values are considered as data that should be optimized by the selected NACEF parameters.

4.2.2 Combined CEF model (σ -CEF-5SL)

In the present work, the combined CEF model proposed by [48,49] is retained in order to describe the σ phase. In this model, a disordering contribution is considered in σ phase in addition to the classical CEF. The Gibbs energy according to the combined CEF with 5 sublattices is given by:

$$G^{\sigma-5SL} = G(x) + G(y) \tag{13}$$

$$G(x) = \sum_i x_i {}^0G_i^{\sigma} + x_i x_j \sum_{\nu=0} (x_i - x_j)^{\nu} {}^{\nu}L \tag{14}$$

$${}^{\nu}L = {}^{\nu}a + {}^{\nu}b\,T \tag{15}$$

$$G(y) = \frac{RT}{\sum_s a^{(s)}} \sum_s a^{(s)} \sum_i y_i^{(s)} \ln y_i^{(s)} + \sum_{i,j,k,l,m} y_i^{(1)} y_j^{(2)} y_k^{(3)} y_l^{(4)} y_m^{(5)} G_{ijklm} \tag{16}$$

$$G_{ijklm} = \Delta H_{ijklm}^{DFT} + b_{ijklm}\,T \tag{17}$$

where ${}^0G_i^{\sigma}$ are the Gibbs energy of the elements in the σ phase structure, ${}^{\nu}L$ is an *v* order interaction parameter. G_{ijklm} is the Gibbs energy of formation of the *ijklm* configuration referred to the elements in the σ phase structure and ΔH_{ijklm}^{DFT} is the corresponding energy which is obtained from DFT calculations. It should be noted that the previous equations lead to obtain for the configuration *ijklm* a formation energy ΔH_{ijklm} given by:

$$\Delta H_{ijklm} = \Delta H_{ijklm}^{DFT} + x_i^{ijklm} x_j^{ijklm} \sum_{\nu=0} \left(x_i^{ijklm} - x_j^{ijklm}\right)^{\nu} {}^{\nu}a \tag{18}$$

where x_i^{ijklm} is the mole fraction of the element *i* of the considered configuration. Thus, the values calculated from the previous formalism become different from those obtained by DFT calculations when the ${}^{\nu}a$ parameters are used. In order to respect the formation energy obtained from the DFT calculations, the end-members of all ordered configurations must be defined as follows:

$$G_{ijklm} = \Delta H_{ijklm}^{DFT} + b_{ijklm}\,T - \left(x_i^{ijklm} x_j^{ijklm} \sum_{\nu=0} \left(x_i^{ijklm} - x_j^{ijklm}\right)^{\nu} {}^{\nu}a \right) \tag{19}$$

Moreover, in the first part of the present work [7], using site fractions notation $y_i^{(s)} = (y_i^{(s)} - x_i) + x_i$, it as been demonstrated that the contribution due to the end-members can be expressed as a sum of a disordered part and an ordered one:

$$\sum_{i,j,k,l,m} y_i^{(1)} y_j^{(2)} y_k^{(3)} y_l^{(4)} y_m^{(5)} G_{ijklm} = G^{\text{dis}}(x) + G^{\text{ord}}(y - x) \tag{20}$$

with the disordered part given by:

$$G^{\text{dis}}(x) = x_i x_j \sum_{\nu=0}^{3} (x_i - x_j)^{\nu} P\nu \tag{21}$$

and where the NACEF parameters $P\nu$ are obtained from the CEF parameters G_{ijklm} from relationships listed in Table 7. Thus, the total disordered contribution becomes:

$$G^{Dis\_\sigma} = x_i x_j \sum_{\nu=0} \left(x_i - x_j\right)^{\nu} {}^{\nu}L^{Dis\_\sigma} \quad (22)$$

$${}^{\nu}L^{Dis\_\sigma} = {}^{\nu}L + P\nu \quad (23)$$

5. Results and discussions

The optimization of the Al–Nb system was carried out using the PARROT module in Thermo-Calc software [51]. The unary descriptions from Dinsdale [52,53] were used for the description of the temperature dependence of the Gibbs energy of the pure elements. The parameters of the thermodynamic model presented above have been assessed in order to obtain the best fit to all the experimental and DFT data first using the σ -CEF-5SL description for the σ phase. Then, the three NACEF models (σ-NACEF-5SL, σ-NACEF-3SL and σ-NACEF-2SL) were used to describe the σ phase and the corresponding parameters have been optimized keeping unchanged the description of the other phases ($A15$, $D0_{22}$, liquid, $A2$, $A1$). The values of all assessed thermodynamic parameters obtained in the present work are summarized in Table 8. The complete thermodynamic databases corresponding to the four descriptions of the σ phase are provided in Thermo-Calc format [54] as supplementary materials. The thermodynamic database corresponding to the σ-NACEF-2SL description is also given in Appendix.

The calculated Al–Nb phase diagrams obtained from the σ-CEF-5SL, σ-NACEF-5SL, σ-NACEF-3SL and σ-NACEF-2SL descriptions of the σ phase are shown in Figs. 3, 4, 5 and 6 respectively on which are compared to the experimental data. In all cases, the calculation reproduces the experimental data of phase boundaries relatively well. Invariant equilibria of the Al–Nb system are summarized in Table 9. The calculated results according to the four versions show also a good agreement with available experimental temperature data.

The site occupancies of Nb calculated at 1198 K in the σ phase are shown in Fig. 7 for the four descriptions along with experimental data obtained by [45,55] at 1123 and 1273 K. For the four versions, the occupancy sequence clearly indicates that Nb has a preference for higher CN sites. Fig. 7 also shows that the σ phase of the Al-Nb system can reasonably be reduced to 2 sublattices since the high CN sites ($4f$, $8i_1$ and $8j$) present very similar behaviors, just like the low CN sites ($2a$ and $8i_2$).

Experimental data for thermodynamic properties of binary Al–Nb alloys reported in literature are based on the KE method [18], EMF method [24] and calorimetry [22,23]. Fig. 8 displays these data along with the corresponding values calculated with the present descriptions based on the four descriptions of the σ phase. One can notice that the calculated results obtained from the four versions are very close and that they are in a good agreement with the experimental data except for the enthalpy of formation at 298.15 K of [18] and [24]. However, it can be noted that these data constitute indirect measurements of the enthalpy at this temperature and that is why they must be considered with a relatively large uncertainty.

Consequently, the results of the DFT calculations constitute the main information retained in our optimization with regard to the enthalpy at low temperature.

For the σ-CEF-5SL description, the DFT values of all the ordered configurations was used to define all end-members and the optimized parameters (see Table 8) are those relative to the disordered contribution $G(x)$ of the combined CEF model (Eqs. 13-15) as well as the temperature dependent parameter b_{ijklm} (Eq. 19) of the $Al^{2a}Nb^{4f}Nb^{8i_1}Al^{8i_2}Nb^{8j}$ configuration.

In the NACEF approach, the DFT values which give the energies of formation of the different compounds are considered as data that should be optimized by the selected NACEF parameters.

Table 4 give the values obtained from the NACEF approach for the σ phase described using the three models (5SL, 3SL and 2SL) and Fig. 9 displays for the 30 stoichiometric σ configurations the DFT results with the corresponding CALPHAD values calculated with the σ-NACEF-5SL description. One can thus observe a very good agreement between these data and this using a development of degree 4 for the σ-NACEF-5SL model. It should also be noted that this result is based on the use of only 30 temperature-independent parameters, which corresponds to the number of configurations taken into account.

Fig. 10 shows for the four descriptions of the σ phase the enthalpy calculated at 1 K with respect to the DFT values of the considered configurations as well as the corresponding disordered contributions which are obtained from the Pv parameters of the three NACEF descriptions (Table 8) and which are given Table 11 for that based on the σ-CEF-5SL model. As comparison, the corresponding results obtained from the σ-CEF-5SL description based on the use of only the 30 compound (end-members) formation energies from DFT are also given Table 11 and displayed on Fig. 10 (a). It can thus be observed that the results obtained for the total enthalpy from the four descriptions are relatively close and that the disordered part constitutes an important contribution of the total enthalpy of the Al-Nb σ phase. Moreover, it appears that the σ-CEF-5SL description requires a larger disordered contribution compared to the three NACEF descriptions.

For the $D0_{22}$ and $A15$ compounds, calculated energies of formation and DFT results are compared Table 10. For the $D0_{22}$ compound, both DFT and CALPHAD results are identical. This is not the case for the $A15$ compound which present a stability domain on the Nb-rich side. The calculated values from DFT for the $A15$ phase do not allow this stability to be achieved, for that, a more negative energy has been considered for its $Nb^{6c}Al^{2a}$ configuration. Fig. 11 shows for the $D0_{22}$ and $A15$ compounds the enthalpy calculated at 1 K with respect to the DFT values of the considered configurations.

The $D0_{22}$ intermediate phase has a body-centred tetragonal structure which is a fcc closed-packed superlattice [42] and the order-disorder transition $D0_{22}$-$A1$ has been easily taken into account in the present work thanks to the NACEF approach. This is highlighted in Fig. 12 which shows the Gibbs energy of formation and the site occupancies of Nb calculated at 934 K, i.e. at a temperature close to that of the peritectic reaction $D0_{22} + L \leftrightarrow A1$. Obviously, the NACEF parameters which describe the disordered excess part of the $D0_{22}$ phase and those for the $A1$ phase are identical (see Table 8).

6. Conclusion

New Al–Nb thermodynamic descriptions has been derived using first-principle calculations and experimental data. DFT calculations have been performed for all the end-member compounds of the σ, *A*15 and $D0_{22}$ phases. The thermodynamic parameters to describe the Gibbs energy of all stable phases of the system have been optimized using the CALPHAD method. The liquid, *A*1 and *A*2 phases have been treated with substitutional solution model and $D0_{22}$ and *A*15 phases was described with a 2SL model in the framework of the NACEF approach. Four different descriptions have been used to describe the σ phase. Firstly, a combined CEF model have been applied for the 5SL description with an original way that allows to respect the DFT results for the ordered configuration energies. Secondly, the σ phase have been modeled by the 5, 3 and 2SL models using the NACEF approach. The four descriptions of the Al-Nb system proposed in the present work which differ only in the used model for σ phase allow to obtain in all cases a good agreement with the various data available and this is obtained with a limited number of assessed parameters. Comparisons between the four proposed descriptions show that the 3SL and 2SL models can reasonably be used to model the σ phase in the Al-Nb system.

Moreover, thanks to the NACEF approach, simplifications can be incorporated into databases in which more complex models are used. These compatibilities can be easily verified in the present work using the NACEF parameters of the 2SL description in the 3 or 5SL models and in the same way, the parameters of the 3SL description in the 5 SL model.

More generally, although NACEF approach is mathematically identical to the widely used CEF, it constitutes a promising way to improve the CEF ability to describe simple or complex phases as shown in this paper.

Declaration of competing interest

The authors declare no conflict of interest.

Acknowledgments

DFT calculations were performed using HPC resources from GENCI-CINES (Grant 2019-096175).

Appendix

Thermodynamic database based on the σ-NACEF-2SL description of the σ phase.

Supplementary material

Thermodynamic databases (TDB files) corresponding to the four descriptions of the σ phase (σ-CEF-5SL, σ-NACEF-5SL, σ-NACEF-3SL and σ-NACEF-2SL) can be found as supplementary material online at:

References

[1] V.T. Witusiewicz, A.A. Bondar, U. Hecht, T.Y. Velikanova, J. Alloys Compd. 472 (2009) 133–161.

[2] C. He, F. Stein, M. Palm, J. Alloys Compd. 637 (2015) 361–375.

[3] F. Stein, C. He, O. Prymak, S. Voß, I. Wossack, Intermetallics 59 (2015) 43–58.

[4] A.A.A.P. da Silva, Thermodynamic modeling and critical experiments on the Al-Fe-Nb system [Thesis]: São Paulo University (USP); 2015.

[5] O. Dovbenko, F. Stein, M. Palm, O. Prymak O, Intermetallics 18(11) (2010) 2191-2207.

[6] A.A.A.P. da Silva, G.C. Coelho, C.A. Nunes, J.M. Fiorani, N. David, M. Vilasi, Materials Research 22(5) (2019) e20190305

[7] J.M. Fiorani, M. Badran, A.A.A.P. da Silva, N. David, M. Vilasi, New Approach to the Compound Energy Formalism (NACEF)-Part I. Thermodynamic modelling of binary phases based on the sublattice model with anti-site type of defects, Calphad, Submitted

[8] V. Glazov, V. Vigdorovich, G. Korolkov, Zhurnal Neorg. Khimii. 4 (1959) 1620–1624.

[9] V. Glazov, G. Lazarev, G. Korolkov, Metalloved. Term. Obrab, Metal. 10 (1959) 48–50.

[10] V.V. Baron, E.M. Savitskii, Neorg. Zh. Khim. 6 (1961) 182–185.

[11] M.J. Richards, Mem. Sci. Rev. Met. 61 (61) (1964) 265–270.

[12] C.E. Lundin, A.S. Yamamoto, Trans. AIME 236 (1966) 863–872.

[13] V. Svechnikov, V. Pan, V. Latysheva, Metallofizika. 22 (1968) 54–61.

[14] A. Wicker, C. Allibert, J. Droile, J. C.R. Acad. Sci. 272C (1971) 1711–1713.

[15] J.L. Jorda, R. Flükiger, J. Muller, J. Less Common Met. 75 (2) (1980) 227–239.

[16] L. Kokot, R. Horyn, N. Iliew, J. Less-Common Met. 44 (1976) 215–219.

[17] E.S.K. Menon, P.R. Subramanian, D.M. Dimiduk, Scr. Metall. Mat. 27 (1992) 265–270.

[18] I. Shilo, H. Franzen, R. Schiffman, J. Electrochem. Soc. 129 (1982) 1608–1613.

[19] Z. Zhu, Y. Du, L. Zhang, H. Chen, H. Xu, C. Tang, J. Alloys Comp. 460 (2008) 632–638.

[20] F. Stein, C. He, I. Wossack, J. Alloys Comp. 598 (2014) 253–265.

[21] G.A. Gelashvili, Z. Dzneladze, Poroshkovaya Metall. 8 (1980) 523–525.

[22] S.V. Meschel, O.J. Kleppa, J. Alloys Comp. 191 (1993) 111–116.

[23] K. Mahdouk, J. Gachon, L. Bouirden, J. Alloys Comp. 268 (1998) 118–121.

[24] P. George, S.C. Parida, R.G. Reddy, Metal. Mater. Trans. B 38B (2007) 85–91.

[25] C. Colinet, A. Pasturel, D.N. Manh, D.G. Pettifor, P. Miodownik, Phys. Rev. B 56(2) (1997) 552–565.

[26] R.E. Watson, M. Weinert, M. Alatalo, Phys. Rev. B 65 (2001) 1-7.

[27] I. Papadimitriou, C. Utton, P. Tsakiropoulos, Comp. Mater. Sci. 107 (2015) 116–121.

[28] A. Pisch, A. Pasturel, Thermochimica Acta 671 (2019) 103–109.

[29] L. Kaufman, H. Nesor, Calphad 2(4) (1978) 325-348.

[30] L. Kaufman, Calphad 15(3) (1991) 251-282.

[31] G. Shao, Intermetallics 12 (2004) 655-664.

[32] U.R. Kattner, W.J. Boettinger, Mater. Sci. Eng. A. 152 (1992) 9–17.

[33] C. Servant, I. Ansara, J. Chim. Phys. 94 (1997) 869–888.

[34] Z.-K. Liu, J. Phase Equilibria Diffusion 30 (2009) 517.

[35] G. Kresse and J. Furthmüller, Phys. Rev. B 54 (1996) 11169.

[36] G. Kresse and D. Joubert, Phys. Rev. 59 (1999) 1758.

[37] J. P. Perdew, K. Burke, and M. Ernzerhof. Phys. Rev. Lett., 77 (1996) 3865.

[38] J. P. Perdew, K. Burke, and M. Ernzerhof. Phys. Rev. Lett., 78 (1997) 1396.

[39] Monkhorst, H. & Pack, Phys. Rev. B, 13 (1976) 5188-5192.

[40] J.C. Crivello, M. Palumbo, T. Abe, J.M. Joubert, Calphad 34 (2010) 487-494.

[41] J.C. Crivello, R. Souques, A. Breidi, N. Bourgeois, J.M. Joubert, Calphad 51 (2015) 233 – 240.

[42] P. Villars, L. Calvert, Pearson's handbook of crystallographic data for intermetallic phases, 2nd ed., Materials Park OH: ASM International, 1991.

[43] P. J. Craievch, M. Weinert, J. M. Sanchez, and R. E. Watson, Phys. Rev. Lett. 72 (1994) 3076.

[44] M. Hillert, J. Alloy. Comp. 320 (2001) 161–176.

[45] J.-M. Joubert, Prog. Mater. Sci. 53 (2008) 528–583.

[46] R. Mathieu, N. Dupin, J.-C. Crivello, K. Yaqoob, A. Breidi, J.-M. Fiorani, N. David, J.-M. Joubert, Calphad 43 (2013) 18–31.

[47] I. Ansara, T.G. Chart, A. Fernandez Guillermet, F.H. Hayes, U.R. Kattner, D.G. Pettifor, N. Saunders, K. Zeng, Calphad 21 (1997) 171–218.

[48] J. Bratberg, B. Sundman, N. Dupin, Application of the combined CEF to the description of the sigma phase in the Pd-Ta system, presented at CALPHAD XXXIX, Korea, 2010.

[49] B. Hallstedt, N. Dupin, M. Hillert, L. Hoglund, H.L. Lukas, J.C. Schuster, N. Solak, Calphad 31 (2007) 28.

[50] Z. Li, H. Mao, P.A. Korzhavyi, M. Selleby, Calphad 52 (2016) 1–7.

[51] Thermo-Calc Software, http://www.thermo-calc.com, visited 11-May-2019.

[52] A.T. Dinsdale, SGTE data for pure elements, Calphad 15 (1991) 317–425.

[53] Scientific Group Thermodata Europe: SGTE, https://www.sgte.net/en/free-puresubstance-database, visited 21-May-2020.

[54] B. Sundman, B. Jansson, J.O. Andersson, Calphad 9 (1985) 153–190.

[55] J.M. Joubert, C. Pommier, E. Leroy, A. Percheron-Guegan, J Alloys Compd. 356–357 (2003) 442–6.

Table 1
Summary of experimental and ab-initio information available for the Al-Nb System.

Information	Reference	Technique	Index
Temperature (Solidus/liquidus)	Jorda et al. [15]	DTA/LTA	A
	Stein et al. [20]	DTA	A
	Wicker et al. [14]	DTA	A
	Witusiewicz et al. [1]	DTA/PA	A
	Zhu et al. [19]	DSC	A
	Lundin and Yamamoto [12]	DTA	B
	Baron and Savitskii [10]	TA	B
	Svechnikov et al. [13]	TA	B
Phase solubility range	Silva et al. [6]	EPMA	A
	Menon et al. [17]	EPMA	A
	Kokot et al. [16]	XRD	A
	Shilo et al. [18]	KE	A
	Jorda et al. [15]	EPMA	A
		MA	B
		XRD	A
		MA	B
	Lundin and Yamamoto [12][(a)]	Hardness	B
		XRD	B
	Svechnikov et al. [13][(a)]	XRD	B
	Glazov et al. [8,9]	Hardness[(b)]	B
Activity	George et al. [24]	EMF	A
	Shilo et al. [18]	KE	A
Enthalpy of formation	Meschel et al. [22]	DRC	A
	Shilo et al. [18]	KE	A
	George et al. [24]	EMF	A
	Mahdouk et al. [23]	DRC	A
	Gelashvili et al. [21]		B
	Colinet et al. [25]	FP	A
	Watson et al. [26]	FP	A
	Papadimitriou et al. [27]	FP	A
	Pisch et al. [28]	FP	A

A – Information used in the optimization
B – Not used
(a) apud Jorda et al. [20]; (b) Solubility of Nb in (Al); DTA: Differential Thermal Analysis; LTA: Levitation Thermal Analysis; PA: Pirani-Alterthum Method; TA: Thermal Analysis; DSC: Differential Scanning Calorimetry; EPMA: Electron Probe Microanalysis; XRD: X-ray Diffractometry; MA: Metallographic Analysis; DRC: Direct Reaction Calorimetry; EMF: Electromotive Force; KE: Knudsen Effusion; FP: First Principles.

Table 2

Crystallographic information of stable solid phases of the Nb-Al system.

(SD=Strukturbericht Designation; PS= Pearson Symbol; SG=Space Group; CN=Coordination Number; WP=Wyckoff position)

Phase	SD	PS	SG	Prototype	Occupation	WP	CN
(Nb)	A2	cI2	$Im\bar{3}m$	W		2*a*	
Nb_3Al	A15	cP8	$Pm\bar{3}n$	Cr_3Si	Al (1)	2*a*	
					Nb (1)	6*c*	
Nb_2Al (σ)	$D8_b$	tP30	P42/mnm	CrFe	Al (1)	2*a*	12
					Nb (1)	$8i_1$	14
					Al (2)	$8i_2$	12
					Nb (2)	4*f*	15
					Nb (3)	8*j*	14
$NbAl_3$	$D0_{22}$	tI8	I4/mmm	$TiAl_3$	Al (1)	2*b*	
					Al (2)	4*d*	
					Nb (1)	2*a*	
(Al)	A1	cF4	$Fm\bar{3}m$	Cu		2*a*	

Table 3

Sublattice models used in literature assessments of the Al-Nb system.

Reference	Sublattice model		
	A15 (Nb_3Al)	σ (Nb_2Al)	$D0_{22}$ ($NbAl_3$)
He et al. [2]	$(Nb)_3(Al,Nb)_1$	$(Nb)_4(Al,Nb)_{16}(Nb,Al)_{10}$	$(Al,Nb)_1(Al,Nb)_3$
Witusiewicz et al. [1]	$(Al,Nb)_3(Al,Nb)_1$	$(Nb)_4(Al,Nb)_{16}(Nb,Al)_{10}$	$(Al,Nb)_1(Al,Nb)_3$
Zhu et al. [19]	$(Nb)_3(Al,Nb)_1$	$(Nb)_4(Al,Nb)_{16}(Nb,Al)_{10}$	$NbAl_3$
Shao [31]	$(Nb)_3(Al,Nb)_1$	$(Nb)_4(Al,Nb)_{18}(Al)_8$	$NbAl_3$
Servant and Ansara [33]	$(Al,Nb)_3(Al,Nb)_1$	$(Nb)_4(Al,Nb)_{16}(Nb,Al)_{10}$	$(Al,Nb)_1(Al,Nb)_3$
Kattner and Boettinger [32]	$(Nb)_3(Al,Nb)_1$	$(Nb)_4(Al,Nb)_{16}(Nb,Al)_{10}$	$(Al,Nb)_1(Al,Nb)_3$
Kaufman [30]	Nb_3Al	(Al,Nb)	$NbAl_3$
Kaufman and Nesor [29]	Nb_3Al	Nb_2Al	$NbAl_3$

Table 4

First-principle enthalpies (J/mol) of σ phase at 0 K. ΔH , resp. ΔH_{σ}, correspond to results referred to fcc Al and bcc Nb, resp. to the σ phase of the pure elements.

Compound							[25]	This Work				
							DFT	DFT	DFT	CALPHAD		
Cn	Occupancy					X(Nb)				NACEF 5SL	NACEF 3SL	NACEF 2SL
	2*a*	4*f*	8i_1	8i_2	8*j*		ΔH	ΔH	ΔH_{σ}	ΔH_{σ}	ΔH_{σ}	ΔH_{σ}
	Al	Al	Al	Al	Al	0		6315				
	Nb	Nb	Nb	Nb	Nb	1		8046				
C1	Nb	Al	Al	Nb	Al	0.333		-14591	-21483	-21467	-21478	-21490
	Al	Nb	Nb	Al	Nb	0.667	-24900	-28638	-36107	-36240	-36193	-36192
C2	Nb	Nb	Al	Nb	Al	0.467		-14495	-21618	-21589	-21616	
	Al	Al	Nb	Al	Nb	0.533		-23866	-31104	-31059	-31018	
C3	Al	Nb	Al	Al	Al	0.133		-6013	-12559	-12685	-12602	
	Nb	Al	Nb	Nb	Nb	0.867		11679	3864	4088	3835	
C4	Al	Nb	Al	Al	Nb	0.4		-26045	-33052	-32938		
	Nb	Al	Nb	Nb	Al	0.6		-3826	-11180	-11365		
C5	Al	Nb	Nb	Al	Al	0.4		-22402	-29409	-29264		
	Nb	Al	Al	Nb	Nb	0.6		-2048	-9402	-9589		
C6	Al	Al	Al	Al	Nb	0.267		-22462	-29239	-29310		
	Nb	Nb	Nb	Nb	Al	0.733		-6246	-13830	-13693		
C7	Al	Al	Nb	Al	Al	0.267		-17138	-23915	-23975		
	Nb	Nb	Al	Nb	Nb	0.733		-5970	-13554	-13462		
C8	Al	Nb	Al	Nb	Al	0.4		-13022	-20029	-19977		
	Nb	Al	Nb	Al	Nb	0.6		-17732	-25086	-25213		
C9	Nb	Nb	Al	Al	Al	0.2		-12350	-19011	-18962		
	Al	Al	Nb	Nb	Nb	0.8		5384	-2316	-2500		
C10	Al	Al	Al	Nb	Al	0.267		-10127	-16904	-16961		
	Nb	Nb	Nb	Al	Nb	0.733		-19379	-26963	-26709		
C11	Nb	Al	Al	Al	Al	0.067		-1733	-8163	-8200		
	Al	Nb	Nb	Nb	Nb	0.933		2135	-5796	-5778		
C12	Nb	Nb	Al	Al	Nb	0.467		-18046	-25169	-25294		
	Al	Al	Nb	Nb	Al	0.533		-6038	-13276	-13091		
C13	Nb	Nb	Nb	Al	Al	0.467		-18947	-26070	-26155		
	Al	Al	Al	Nb	Nb	0.533		-9699	-16937	-16715		
C14	Nb	Al	Al	Al	Nb	0.333		-14602	-21494	-21363		
	Al	Nb	Nb	Nb	Al	0.667		-7362	-14831	-15021		
C15	Nb	Al	Nb	Al	Al	0.333		-15820	-22712	-22590		
	Al	Nb	Al	Nb	Nb	0.667		-11338	-18807	-18883		

Table 5

First-principle enthalpies (kJ/mol) of A15 phase at 0 K. The reported values obtained in the present work from DFT calculation are compared with DFT literature data. ΔH , resp. ΔH_{A15} , correspond to results referred to fcc Al and bcc Nb, resp. to the A15 phase of the pure elements.

Occupancy		X(Nb)	This Work		[25]
6*c*	2*a*		ΔH	ΔH_{A15}	ΔH
Al	Al	0	7.537	0	
Nb	Nb	1	10.153	0	
Al	Nb	0.25	-6.563	-14.754	
Nb	Al	0.75	-17.471	-26.969	-19

Table 6

First-principle enthalpies (kJ/mol) of $D0_{22}$ phase at 0 K. The reported values obtained in the present work from DFT calculation are compared with DFT literature data. ΔH , resp. ΔH_{D022} , correspond to results referred to fcc Al and bcc Nb, resp. to the $D0_{22}$ phase of the pure elements. Figures in italics correspond to the $\left(H_i^{FCC} - H_i^{SER}\right)$ values taken from the SGTE unary database [52,53] to which is added 1 J/mol.

Occupancy			X(Nb)	This Work		[25]	[26]	[27]	[28]
2*b*	4*d*	2*a*		ΔH	ΔH_{D022}	ΔH	ΔH	ΔH	ΔH
Al	Al	Al	0	*0.001*	0				
Nb	Nb	Nb	1	*13.501*	0				
Al	Al	Nb	0.25	-41.559	-44.935	-41.5	-39.6	-47.4	-40.8
Nb	Nb	Al	0.75	-6.345	-16.471				

Table 7

Relationships between the NACEF parameters of the disordered contribution and the end-members of the 5SL model in CEF description of the σ phase (see Eqs. 19,20).

$$P0 = \tfrac{1}{8}\big(G_{AAAAB} + G_{BBBBA} + G_{AAABA} + G_{BBBAB} + G_{AABAA} + G_{BBABB} + G_{ABAAA} + G_{BABBB} + G_{BAAAA} + G_{ABBBB}$$
$$+ G_{AAABB} + G_{BBBAA} + G_{AABAB} + G_{BBABA} + G_{ABAAB} + G_{BABBA} + G_{BAAAB} + G_{ABBBA} + G_{AABBA} + G_{BBAAB}$$
$$+ G_{ABABA} + G_{BABAB} + G_{BAABA} + G_{ABBAB} + G_{ABBAA} + G_{BAABB} + G_{BABAA} + G_{ABABB} + G_{BBAAA} + G_{AABBB}\big)$$

$$P1 = \tfrac{1}{8}\big(3G_{AAAAB} - 3G_{BBBBA} + 3G_{AAABA} - 3G_{BBBAB} + 3G_{AABAA} - 3G_{BBABB} + 3G_{ABAAA} - 3G_{BABBB} + 3G_{BAAAA} - 3G_{ABBBB}$$
$$+ G_{AAABB} - G_{BBBAA} + G_{AABAB} - G_{BBABA} + G_{ABAAB} - G_{BABBA} + G_{BAAAB} - G_{ABBBA} + G_{AABBA} - G_{BBAAB}$$
$$+ G_{ABABA} - G_{BABAB} + G_{BAABA} - G_{ABBAB} + G_{ABBAA} - G_{BAABB} + G_{BABAA} - G_{ABABB} + G_{BBAAA} - G_{AABBB}\big)$$

$$P2 = \tfrac{1}{8}\big(3G_{AAAAB} + 3G_{BBBBA} + 3G_{AAABA} + 3G_{BBBAB} + 3G_{AABAA} + 3G_{BBABB} + 3G_{ABAAA} + 3G_{BABBB} + 3G_{BAAAA} + 3G_{ABBBB}$$
$$- G_{AAABB} - G_{BBBAA} - G_{AABAB} - G_{BBABA} - G_{ABAAB} - G_{BABBA} - G_{BAAAB} - G_{ABBBA} - G_{AABBA} - G_{BBAAB}$$
$$- G_{ABABA} - G_{BABAB} - G_{BAABA} - G_{ABBAB} - G_{ABBAA} - G_{BAABB} - G_{BABAA} - G_{ABABB} - G_{BBAAA} - G_{AABBB}\big)$$

$$P3 = \tfrac{1}{8}\big(G_{AAAAB} - G_{BBBBA} + G_{AAABA} - G_{BBBAB} + G_{AABAA} - G_{BBABB} + G_{ABAAA} - G_{BABBB} + G_{BAAAA} - G_{ABBBB}$$
$$- G_{AAABB} + G_{BBBAA} - G_{AABAB} + G_{BBABA} - G_{ABAAB} + G_{BABBA} - G_{BAAAB} + G_{ABBBA} - G_{AABBA} + G_{BBAAB}$$
$$- G_{ABABA} + G_{BABAB} - G_{BAABA} + G_{ABBAB} - G_{ABBAA} + G_{BAABB} - G_{BABAA} + G_{ABABB} - G_{BBAAA} + G_{AABBB}\big)$$

Table 8

Thermodynamic parameters for the phases of the Al–Nb system obtained in this work (J/mol). The parameters for the pure elements in fcc, bcc and liquid structure where taken form the SGTE unary database [52,53].

Liquid	A2	A1
(Al,Nb)	(Al,Nb)	(Al,Nb)
${}^0G_{Al}^{LIQ} = GLIQAL$	${}^0G_{Al}^{A2} = GBCCAL$	${}^0G_{Al}^{A1} = GHSERAL$
${}^0G_{Nb}^{LIQ} = GLIQNB$	${}^0G_{Nb}^{A2} = GHSERNB$	${}^0G_{Nb}^{A1} = GFCCNB$
${}^0L_{Al,Nb}^{LIQ} = -100610 + 21.5T$	${}^0L_{Al,Nb}^{A2} = -94212 + 15.567T$	${}^0L_{Al,Nb}^{A1} = -62501 + 3.953T$
	${}^1L_{Al,Nb}^{A2} = -14268$	${}^1L_{Al,Nb}^{A1} = -45024$

A15	$D0_{22}$	σ-CEF-5SL
$(Al,Nb)_3^{6c}(Al,Nb)_1^{2a}$	$(Al,Nb)_3^{2b+4d}(Al,Nb)_1^{2a}$	$(A,B)_2^{2a}(A,B)_4^{4f}(A,B)_8^{8i_1}(A,B)_8^{8i_2}(A,B)_8^{8j}$
${}^0G_{Al}^{A15} = GHSERAL + 7537$	${}^0G_{Al}^{DO_{22}} = GHSERAL + 1$	${}^0G_{Al}^{\sigma} = GHSERAL + 6315$
${}^0G_{Nb}^{A15} = GHSERNB + 10153$	${}^0G_{Nb}^{DO_{22}} = GFCCNB + 1$	${}^0G_{Nb}^{\sigma} = GHSERNB + 8046$
$P0 = -86621$	$P0 = -62501 + 3.953T$	ΔH_{ijklm}^{DFT} of all compounds
$P10 = 1428$	$P1 = -45024$	${}^0L = -91616 + 15.827T$
$P11 = -9032$	$P30 = 10011$	${}^1L = -57905 + 5.458T$
$P12 = -36424 + 1.278T$	$P40 = -18984 + 6.202T$	${}^2L = 32037 - 37.377T$
$P20 = -10707$		${}^3L = 34266$
		$b_{Al:Nb:Nb:Al:Nb} = 0.226T$

σ NACEF

${}^0G_{Al}^{\sigma} = GHSERAL + 6315$ ${}^0G_{Nb}^{\sigma} = GHSERNB + 8046$

σ-NACEF-5SL	σ-NACEF-3SL	σ-NACEF-2SL
$(A,B)_2^{2a}(A,B)_4^{4f}(A,B)_8^{8i_1}(A,B)_8^{8i_2}(A,B)_8^{8j}$	$(A,B)_4^{4f}(A,B)_{16}^{8i_1+8j}(A,B)_{10}^{2a+8i_2}$	$(A,B)_{20}^{4f+8i_1+8j}(A,B)_{10}^{2a+8i_2}$
$P0 = -78940 + 17.833T$	$P0 = -74106 + 18.921T$	$P0 = -72707 + 18.903T$
$P1 = -31868$	$P1 = -30058$	$P1 = -24137$
$C1P10 = -12995$	$C1P10 = -21375$	$C1P10 = -21807$
$C4P10 = 12758$		
$C6P10 = 3540$		
$C10P10 = 8336$		
$C1P11 = 4.951T$	$C1P11 = -18298 + 5.664T$	$C1P11 = -20929 + 5.676T$
$C2P11 = -5983$		
$C1P20 = -12556$	$C1P20 = -11687$	$C1P20 = -13402$
	$C2P20 = -3596$	
$C3P20 = 4637$	$C3P20 = 7518$	
$C5P20 = 6544$		
$C6P20 = -6866$		
$C7P20 = -4226$		
$C9P20 = -3475$		
$C12P20 = 6853$		
$C1P30 = 3998$	$C1P30 = 9393$	$C1P30 = 12668$
	$C2P30 = 6785$	
	$C3P30 = 1313$	

$C5P30 = 7031$

$C6P30 = -6053$

$C7P30 = 2382$

$C9P30 = 3237$

$C10P30 = -978$

$C11P30 = 4445$

$C12P30 = -5669$

$C13P30 = -2362$

$C14P30 = -2012$

$C15P30 = 4723$

$C1P31 = 7508$ $C1P31 = 18173$ $C1P31 = 18774$

$C2P40 = 6979$

$C8P40 = -2663$

$C11P40 = -2039$

$C14P40 = 1561$

Table 9

Invariant equilibria calculated in this work (TW) compared with experimental data.

Invariant reaction φ_1 , φ_2 , φ_3	T (K)	Nb at.%			Ref.
		φ_1	φ_2	φ_3	
A2 + L ↔ A15	2335	80.3	73.0	78.7	σ-CEF-5SL
	2335	80.3	73.0	78.7	σ-NACEF-5SL
	2335	80.3	73.0	78.7	σ-NACEF-3SL
	2335	80.3	73.0	78.7	σ-NACEF-2SL
	2336±15				[1]
	2333±10				[15]
A15 + L ↔ σ	2205	75.9	64.5	70.5	σ-CEF-5SL
	2206	75.9	64.5	68.5	σ-NACEF-5SL
	2206	75.9	64.5	68.4	σ-NACEF-3SL
	2206	75.9	64.5	68.4	σ-NACEF-2SL
	2208±7				[1]
	2213±10				[15]
L ↔ $D0_{22}$	1985	25.2	25.2		σ-CEF-5SL
	1985	25.2	25.2		σ-NACEF-5SL
	1985	25.2	25.2		σ-NACEF-3SL
	1985	25.2	25.2		σ-NACEF-2SL
	1986±4				[1]
	1953				[15]
	2000				[20]
L ↔ σ + $D0_{22}$	1848	42.0	52.3	25.8	σ-CEF-5SL
	1849	42.0	54.7	25.8	σ-NACEF-5SL
	1849	41.9	54.5	25.8	σ-NACEF-3SL
	1849	41.9	54.7	25.8	σ-NACEF-2SL
	1845±7				[1]
	1863±5				[15]
$D0_{22}$ + L ↔ A1	934.5	25.0	0.004	0.15	σ-CEF-5SL
	934.5	25.0	0.004	0.15	σ-NACEF-5SL
	934.5	25.0	0.004	0.15	σ-NACEF-3SL
	934.5	25.0	0.004	0.15	σ-NACEF-2SL
	934.6±0.5				[19]
	934.6±0.5				[15]
	930±5				[1]
L ↔ A1 + $D0_{22}$	933				[10]
A15 ↔ σ + A2	497	77.8	66.7	98.9	σ-CEF-5SL
	573	78.3	67.1	98.5	σ-NACEF-5SL
	558	78.2	67.2	98.5	σ-NACEF-3SL
	558	78.2	67.1	98.5	σ-NACEF-2SL

Table 10

Comparison of the DFT energies values (ΔH_{φ}^{DFT}) with the values ($\Delta H_{\varphi}^{Calc.}$) calculated in the present CALPHAD assessment for the ordered configurations of the A15 and $D0_{22}$ phases (kJ/mol)

φ phases	Compounds	ΔH_{φ}^{DFT}	$\Delta H_{\varphi}^{Calc.}$
A15	Al_3Nb_1	-14.754	-14.754
	Nb_3Al_1	-26.969	-30.110
$D0_{22}$	Al_3Nb_1	-44.935	-44.935
	Nb_3Al_1	-16.471	-16.471

Table 11

${}^{\nu}L^{Dis-\sigma}$ parameters (J/mol) of the σ phase disordered part and obtained from Eqs. 22-23 in the σ-CEF-5SL description. The column σ-CEF-5SL^{EM} gives the parameters of the disordered contributions obtained using only the 30 compound (end-members) formation energies from DFT, i.e. when all the ${}^{\nu}L$ parameters are zero.

σ-CEF-5SL			σ-CEF-5SL^{EM}
${}^{\nu}L$	$P\nu$	${}^{\nu}L^{Dis-\sigma} = {}^{\nu}L + P\nu$	${}^{\nu}L^{Dis-\sigma}$
${}^{0}L = -91616 + 15.827\,T$	$P0 = -3941 + 0.02825\,T$	${}^{0}L^{Dis-\sigma} = -95557 + 15.85525\,T$	${}^{0}L^{Dis-\sigma} = -70769$
${}^{1}L = -57905 + 5.458\,T$	$P1 = 1905 - 0.02825\,T$	${}^{1}L^{Dis-\sigma} = -56000 + 5.42975\,T$	${}^{1}L^{Dis-\sigma} = -17678$
${}^{2}L = 32037 - 37.377\,T$	$P2 = -7135 - 0.02825\,T$	${}^{2}L^{Dis-\sigma} = 24902 - 37.40525\,T$	${}^{2}L^{Dis-\sigma} = -2760.5$
${}^{3}L = 34266$	$P3 = -266 + 0.02825\,T$	${}^{3}L^{Dis-\sigma} = 34000 + 0.02825\,T$	${}^{3}L^{Dis-\sigma} = -427.5$

Please note that all figures should be printed in color.

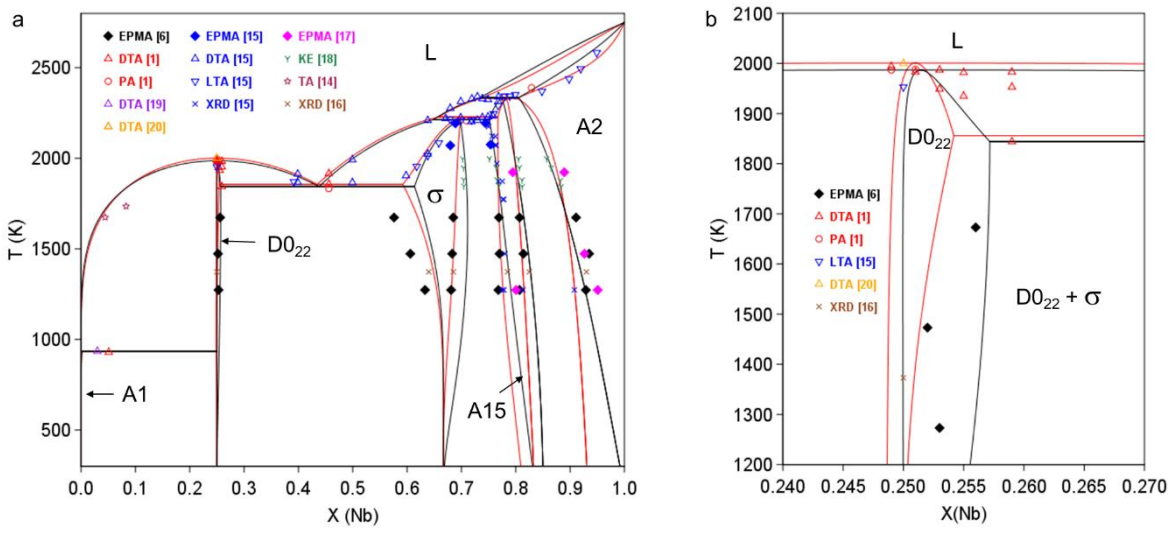

Fig. 1. Calculated Al–Nb phase diagram using the descriptions from Witusiewicz et al. [1] (black lines) and He et al. [2] (red lines) along with experimental data: (a) entire diagram; (b) enlarged part in the vicinity of $D0_{22}$ phase.

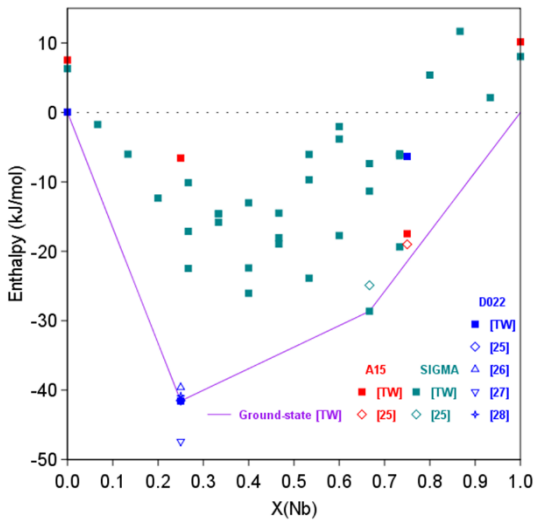

Fig. 2. First-principle enthalpies of formation at 0 K of the ordered configurations of the σ, $D0_{22}$ and A15 phases obtained in this work [TW] and from literature. Reference states are the fcc-Al and bcc-Nb.

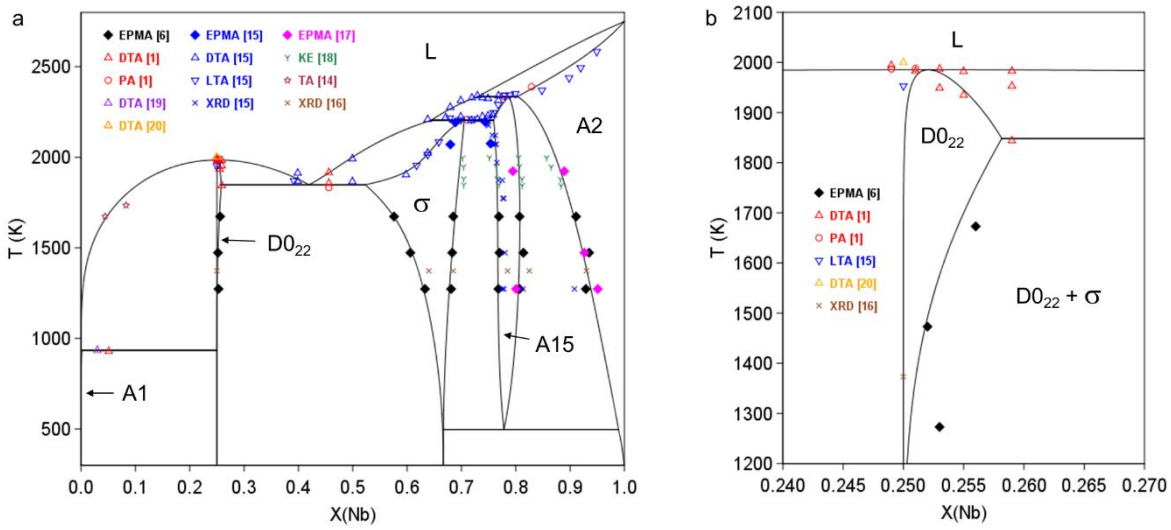

Fig. 3. Calculated Al–Nb phase diagram obtained from this work using the σ-CEF-5SL model for the σ phase description: (a) entire diagram; (b) enlarged part in the vicinity of $D0_{22}$ phase.

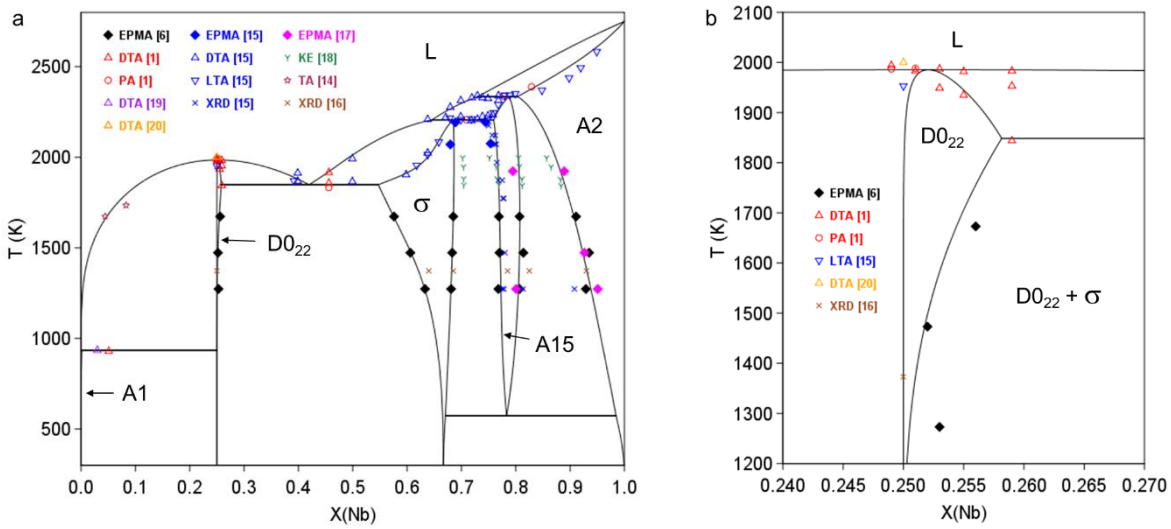

Fig. 4. Calculated Al–Nb phase diagram obtained from this work using the σ-NACEF-5SL model for the σ phase description: (a) entire diagram; (b) enlarged part in the vicinity of $D0_{22}$ phase.

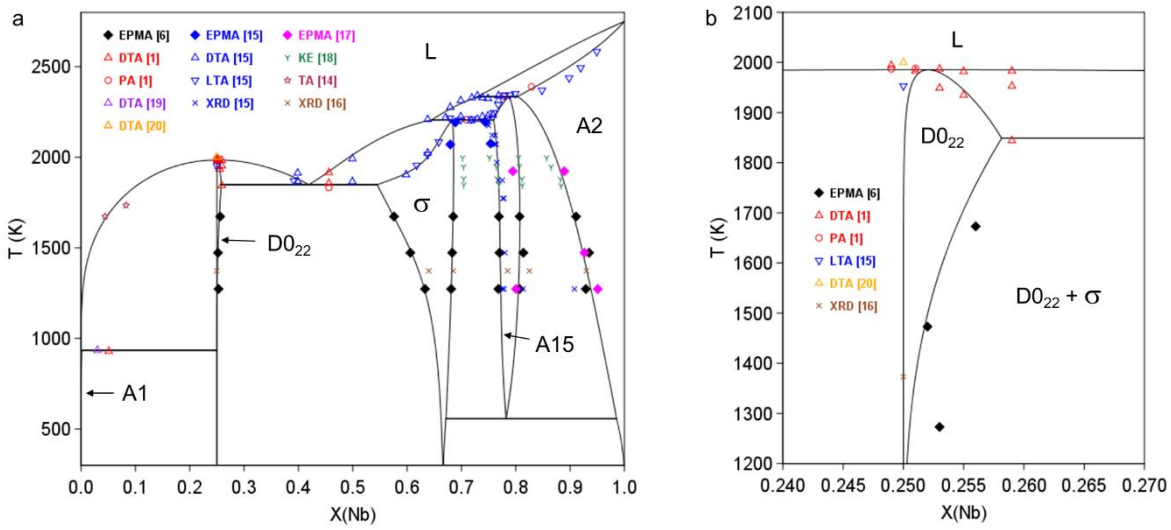

Fig. 5. Calculated Al–Nb phase diagram obtained from this work using the σ-NACEF-3SL model for the σ phase description: (a) entire diagram; (b) enlarged part in the vicinity of $D0_{22}$ phase.

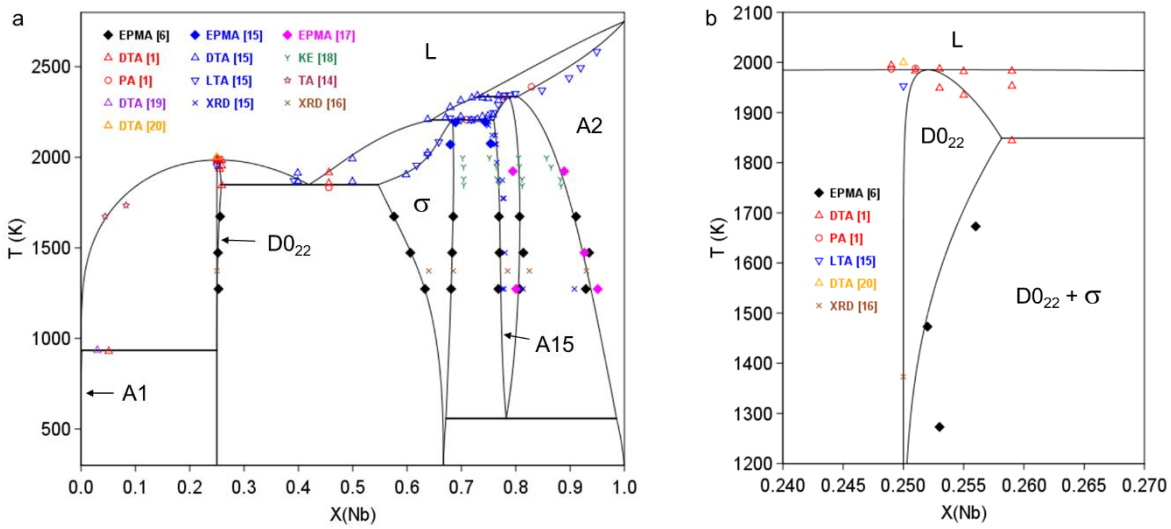

Fig. 6. Calculated Al–Nb phase diagram obtained from this work using the σ-NACEF-2SL model for the σ phase description: (a) entire diagram; (b) enlarged part in the vicinity of $D0_{22}$ phase.

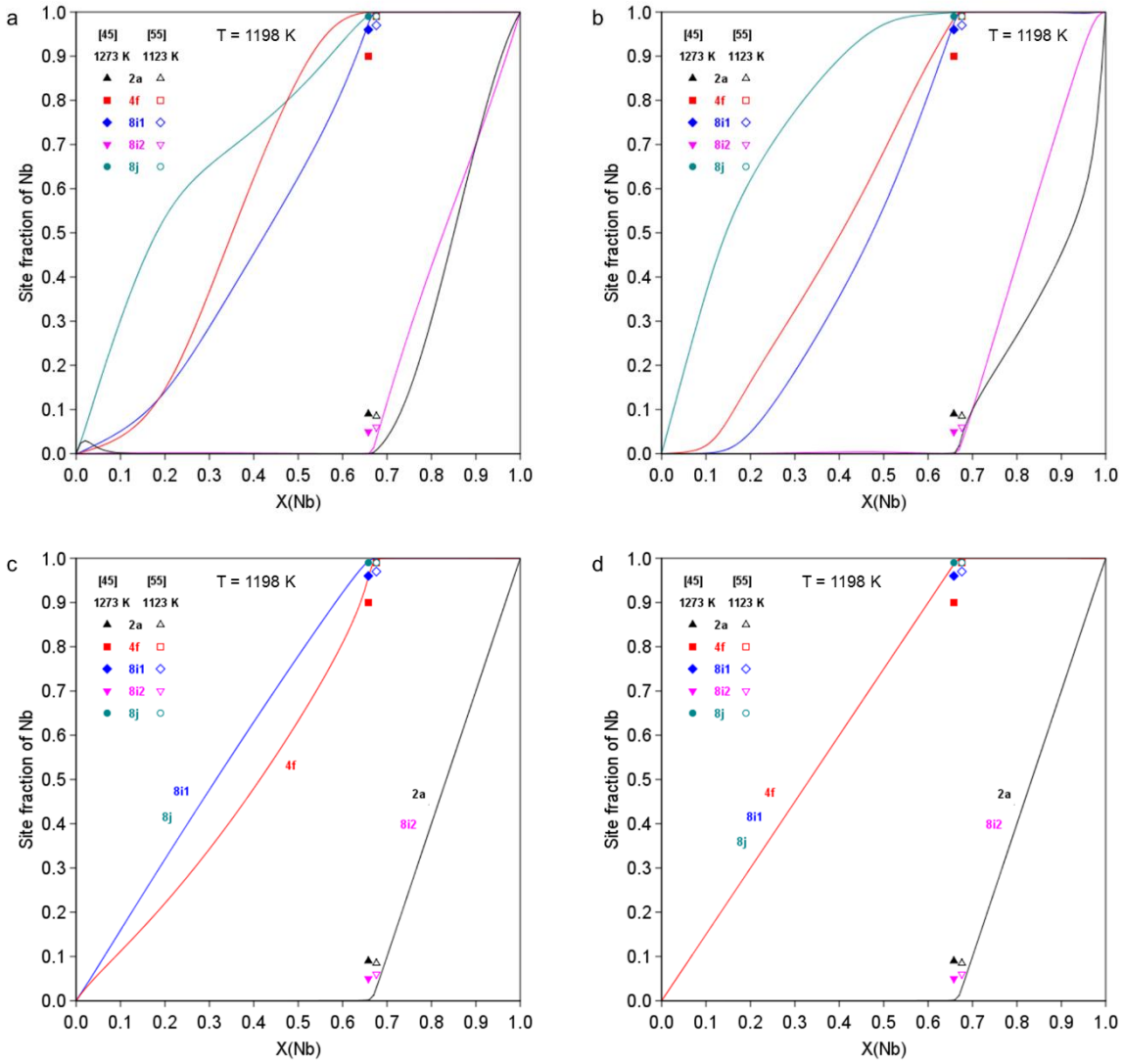

Fig. 7. Calculated site occupancies of the σ phase at 1198 K obtained from the σ-CEF-5SL (a), σ-NACEF-5SL (b), σ-NACEF-3SL (c) and σ-NACEF-2SL (d) descriptions. Experimental data at 1273 K [45] and 1123 K [55] are also plotted for comparison.

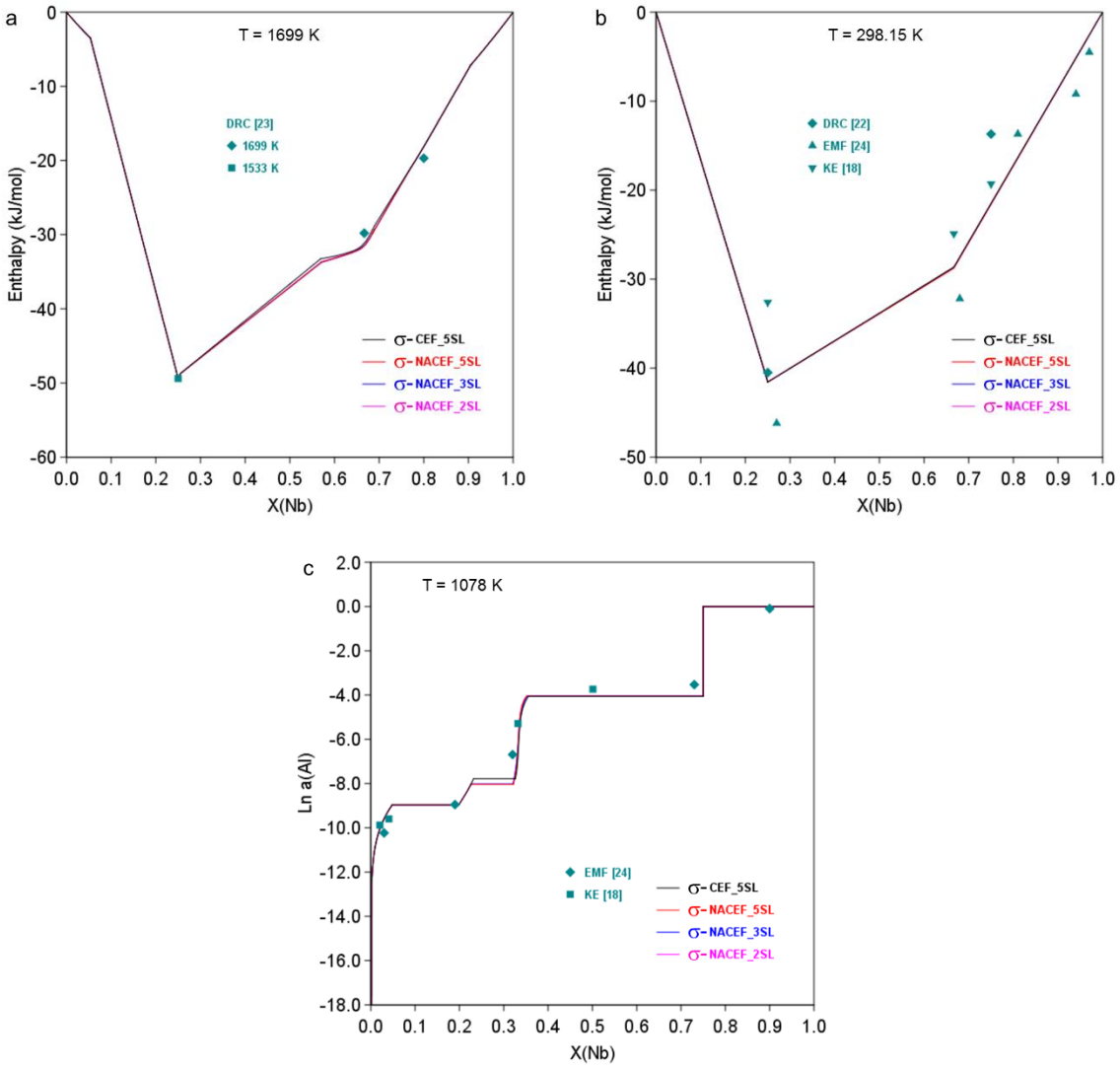

Fig. 8. Thermodynamic properties of the Al-Nb system obtained in this work from the four descriptions of the σ phase (σ-CEF-5SL, σ-NACEF-5SL, σ-NACEF-3SL and σ-NACEF-2SL) descriptions compared with experimental data:
(a) Enthalpy of formation at 1699 K (reference states are bcc-Nb and liquid-Al),
(b) Enthalpy of formation at 298 K (reference states are bcc-Nb and fcc-Al).
(c) Calculated activity of Al at 1078 K referred to liquid.

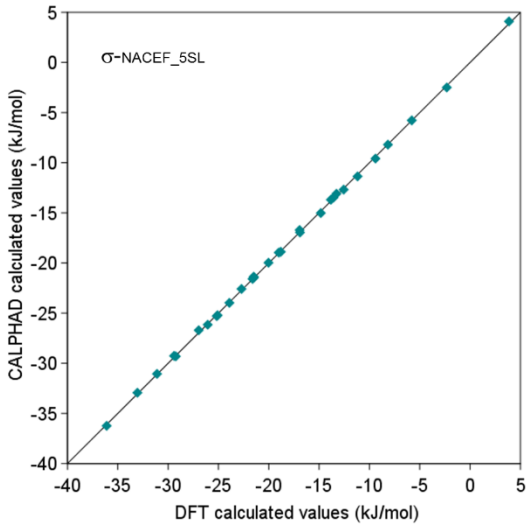

Fig. 9. Formation energies of the 30 stoichiometric σ configurations from the pure elements in the σ structure. For each compound, the *x* coordinate corresponds to the DFT results [22], and the *y* coordinate corresponds to the CALPHAD values calculated with the σ-NACEF-5SL description.

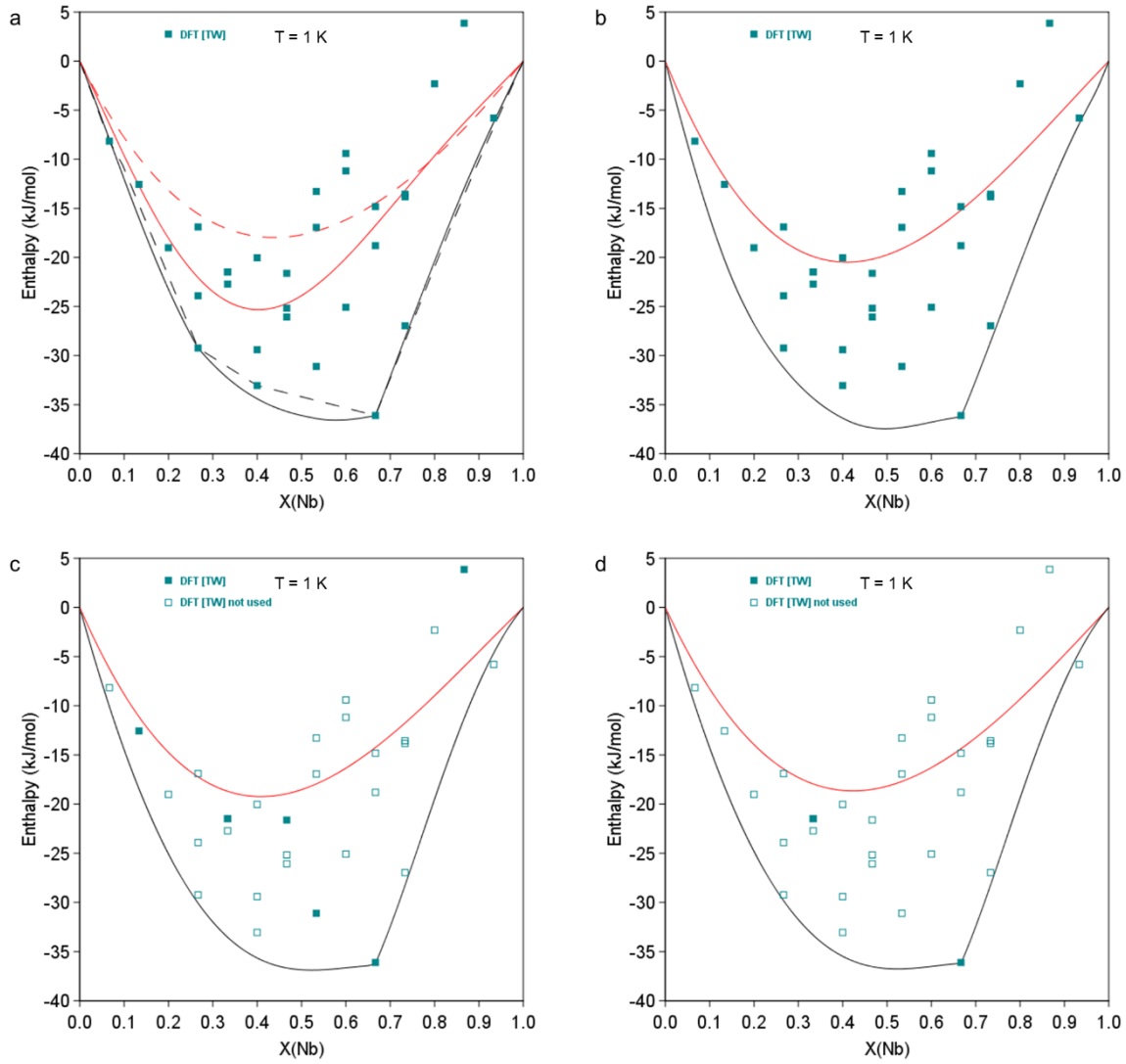

Fig. 10. Enthalpies of formation (black line) of the σ phase obtained at 1 K from the σ-CEF-5SL (a), σ-NACEF-5SL (b), σ-NACEF-3SL (c) and σ-NACEF-2SL (d) descriptions compared with DFT results obtained at 0 K. The red lines represent the corresponding disordered contributions. In the case of the σ-CEF-5SL (a) description are also shown in black and red dashed lines the corresponding results obtained using only the 30 compound formation energies from DFT. Reference states are σ-Al and σ-Nb.

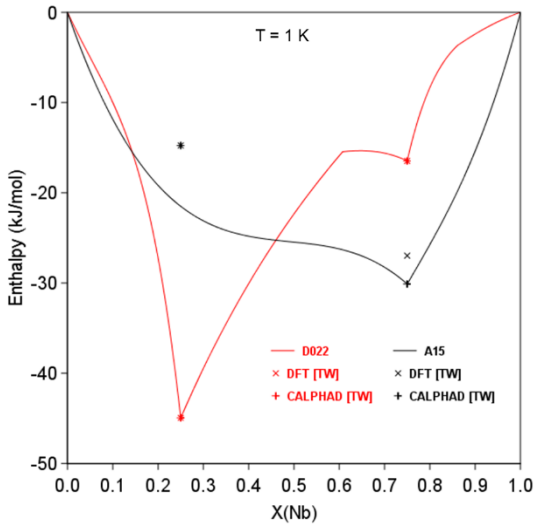

Fig. 11. Calculated enthalpies of formation at 1 K (lines) and compound energies (symbols) for the $D0_{22}$ and A15 phases. Reference states are the corresponding phase for the pure elements.

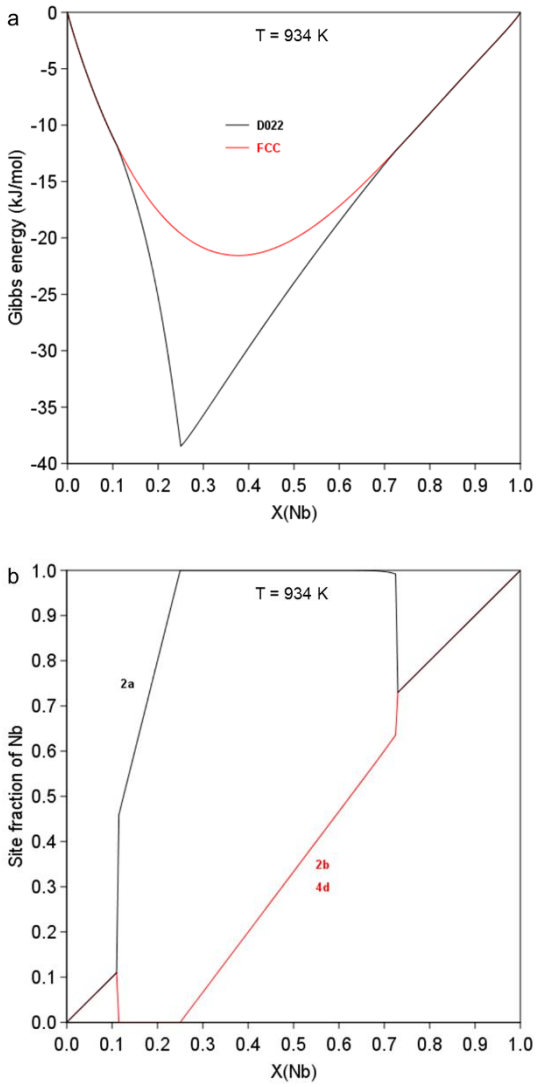

Fig. 12. Calculated Gibbs energy of formation (a) and site occupancies (b) of the $D0_{22}$ and A1 phases at 934 K. Reference states are fcc-Al and fcc-Nb at the current temperature.